

A comprehensive comparison between APOGEE and LAMOST Radial Velocities and Atmospheric Stellar Parameters

B. Anguiano,^{1,2} S. R. Majewski,¹ C. Allende-Prieto,^{3,4} S. Meszaros,^{5,6} H. Jönsson,⁷ D. A. García-Hernández,^{3,4} R. L. Beaton,^{8,9,*,**} G. S. Stringfellow,¹⁰ K. Cunha,^{11,12} V. V. Smith¹³

¹ Department of Astronomy, University of Virginia, Charlottesville, VA 22904-4325, USA
e-mail: ba7t@virginia.edu

² Department of Physics & Astronomy, Macquarie University, Balaclava Rd, NSW 2109, Australia

³ Instituto de Astrofísica de Canarias (IAC), E-38205 La Laguna, Tenerife, Spain

⁴ Universidad de La Laguna (ULL), Departamento de Astrofísica, E-38206 La Laguna, Tenerife, Spain

⁵ ELTE Eötvös Lorand University, Gothárd Astrophysical Observatory, Szombathely, Hungary

⁶ Premium Postdoctoral Fellow of the Hungarian Academy of Sciences

⁷ Lund Observatory, Department of Astronomy and Theoretical Physics, Lund University, Box 43, SE-22100 Lund, Sweden

⁸ Department of Astrophysical Sciences, Princeton University, 4 Ivy Lane, Princeton, NJ 08544

⁹ The Observatories of the Carnegie Institution for Science, 813 Santa Barbara Street, Pasadena, California 91101, USA

¹⁰ Center for Astrophysics and Space Astronomy, University of Colorado, 389 UCB, Boulder, CO 80309-0389, USA

¹¹ University of Arizona, Tucson, AZ 85719, USA

¹² Observatório Nacional, São Cristóvão, Rio de Janeiro, Brazil

¹³ National Optical Astronomy Observatories, Tucson, AZ 85719 USA

Received May 7, 2018; accepted Jul 18, 2018

ABSTRACT

Aims. We undertake a critical and comprehensive comparison of the radial velocities and the main stellar atmospheric parameters for stars in common between the latest data releases from the APOGEE and the LAMOST surveys.

Methods. APOGEE is a high-resolution, high-signal-to-noise ratio spectroscopic survey, part of the SDSS. The latest data release, SDSS DR14, comprises APOGEE spectra for 263,444 stars, together with main stellar parameters and individual abundances for up to 20 chemical species. LAMOST is a low-resolution optical spectroscopic survey, where LAMOST DR3 contains 3,177,995 stars.

Results. There is a total of 42,420 dwarfs/giants stars in common between the APOGEE DR14 - LAMOST DR3 stellar catalogs. A comparison between APOGEE and LAMOST RVs shows an offset of $4.54 \pm 0.03 \text{ km s}^{-1}$, with a dispersion of 5.8 km s^{-1} , in the sense that APOGEE RVs are larger. We observe a small offset in the effective temperatures of about 13 K, with a scatter of 155 K. A small offset in [Fe/H] of about 0.06 dex together with a scatter of 0.13 dex is also observed. We notice that the largest offset between the surveys occurs in the surface gravities. Using only surface gravities in calibrated red giants from APOGEE DR14, where there are 24,074 stars in common, a deviation of 0.14 dex is found with substantial scatter (0.25 dex). There are 17,482 red giant stars in common between APOGEE DR14 and those in LAMOST tied to APOGEE DR12 via *the Cannon*. There is generally good agreement between the two data-sets. However, we find dependencies of the differences of the stellar parameters on effective temperature. For metal-rich stars, a different trend for the [Fe/H] discrepancies is found. Surprisingly, we see no correlation between the internal APOGEE DR14 - DR12 differences in T_{eff} and those in DR14 - LAMOST tied to DR12, where a correlation should be expected since LAMOST has been calibrated to APOGEE DR12. We also find no correlation between the [Fe/H] discrepancies, suggesting that LAMOST/*Cannon* is not well coupled to the APOGEE DR12 stellar parameters scale. An [Fe/H] dependence between the stellar parameters in APOGEE DR12 and those in DR14 is reported. We find a weak correlation in the differences between APOGEE DR14 - DR12 and LAMOST on DR12 surface gravity for stars hotter than 4800 K and in the log g range between 2.0 and 2.8 dex. We do not observe an [Fe/H] dependency in the gravity discrepancies.

Key words. surveys – stars: fundamental parameters – asteroseismology

1. Introduction

The structure of a stellar atmosphere is principally determined by three atmospheric parameters; the effective temperature, the surface gravity and the chemical enrichment level. These parameters are the foundation of the physical interpretation of stellar spectra and, together with radial velocities, the most important measurements sought after for the different scien-

tific goals of current massive stellar spectroscopic surveys. Hence automated stellar parameter pipelines (SPPs) and their validation are extremely important for the scientific exploitation of these survey data (Lee et al. 2008, Smolinski et al. 2011, Anguiano et al. 2015).

In this study we focus on the latest data releases from two large ongoing observational programs, the APOGEE (Majewski et al. 2017) and LAMOST (Zhao et al. 2012) surveys. Our main goal is to work out a comprehensive comparison between the radial velocities and the main stellar atmosphere pa-

* Hubble Fellow

** Carnegie-Princeton Fellow

rameters for the stars in common between the two surveys. This comparison can illuminate how similar the stellar velocity and atmospheric parameters are for each survey, to evaluate random errors, and to find systematic effects within the data-sets. This comparison is especially helpful because LAMOST observes in the optical at medium-low resolution, while APOGEE survey works in the H -band at higher resolving power, and they use different analysis methodologies to obtain the information from the observed spectra.

Data-driven methods for measuring stellar parameters, like *The Cannon* (Ness et al. 2015), have been developed in the recent years to bring surveys with disjoint wavelength coverage and different resolving power onto the same scale using a training sample observed by both spectroscopic programs. Recently, Ho et al. (2017) used *The Cannon* to transfer information from APOGEE Data Release 12 (DR12) to determine precise stellar parameters from the spectra of 450,000 LAMOST giants. In this study we also use the intersection between the APOGEE and LAMOST data-sets to compare the more recent Data Release 14 (DR14) of APOGEE to the LAMOST giants calibrated to the APOGEE DR12 scale. Moreover, asteroseismology in the *Kepler* field (Borucki et al. 2010) provides accurate surface gravities for red giants. Using the overlap between APOGEE and LAMOST, and also the photometric survey SAGA (Casagrande et al. 2014) in the *Kepler* field, we are able to quantify the discrepancies between surface gravity derived from spectroscopic analysis and those from asteroseismology (Pinsonneault et al. 2014).

This paper is organized as follows. In Section 2 we describe the APOGEE and LAMOST surveys together with the stellar catalog of common stars. Sky coverage, magnitude range, signal-to-noise ratio, radial velocities and stellar parameters together with their uncertainties and systematic effects are discussed in detail. The APOGEE and LAMOST targets in the *Kepler* field are described in Section 3. We emphasize that in Section 2 and 3 we compare APOGEE with LAMOST's own pipelines. In Section 4 we study the discrepancies between APOGEE and LAMOST calibrated to the APOGEE DR12 stellar parameters scale via *The Cannon*. We present our conclusions and how this massive overlap between the surveys presents an opportunity to build a robust training data-set for data-driven methods for measuring stellar parameters in Section 5.

2. The APOGEE-LAMOST stellar catalog

The Apache Point Observatory Galaxy Evolution Experiment (APOGEE), and its successor APOGEE-2, is a high-resolution ($R \sim 22,500$), high-signal-to-noise ($\text{SNR} > 100$ per half resolution element) spectroscopic survey using the 2.5-meter Sloan telescope in the Northern Hemisphere and the du Pont telescope at Las Campanas Observatory for the Southern Hemisphere (Majewski et al. 2017). The survey operates in the near-infrared H -band, and can take 300 spectra simultaneously (Wilson et al. 2010). The latest APOGEE data release, DR14 (Abolfathi et al. 2018), comprises spectra for 263,444 stars, together with main stellar parameters and individual abundances for up to 15 chemical species.

The Large sky Area Multi-Object Spectroscopic Telescope (LAMOST) is a national scientific research facility operated by the Chinese Academy of Sciences. LAMOST is a low-resolution ($R \sim 1800$), optical (3650 - 9000 Å) spectroscopic survey in the Northern Hemisphere. Using a modified Schmidt telescope, LAMOST can observe up to 4000 objects simultaneously over a 20 sq. deg field-of-view. The LAMOST Experiment

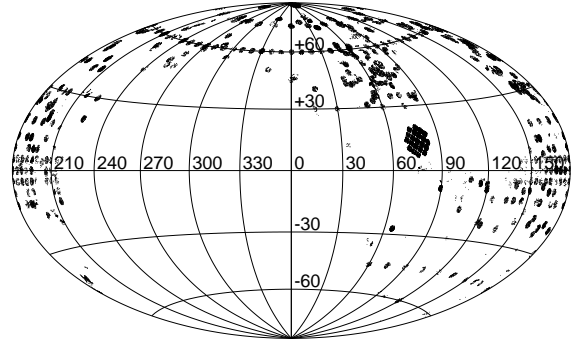


Fig. 1. A Hammer-Aitoff projection in Galactic coordinates (l, b) of the APOGEE-LAMOST stellar catalog distribution. Most of the stars are in the North Galactic Pole and in the Galactic anti-center. Note also the *Kepler* field around $l \sim 70^\circ$, $b \sim +15^\circ$

for Galactic Understanding and Exploration (LEGUE) is an ongoing Galactic survey with a present sample of more than 5 million stellar spectra (Deng et al. 2012). LAMOST DR3¹ published 3,177,995 stars in this catalog, including 45,826 A type stars, 988,947 F type stars, 1,600,512 G type stars and 542,710 K type stars. These objects are selected with the criteria of having a SNR in the g band larger than 6 obtained during dark nights, and SNR in g band larger than 15 obtained during bright nights.

Using a comparison of positions in equatorial coordinates between the surveys, we selected stars where $(\Delta\alpha^2 + \Delta\delta^2)^{1/2} < 3$ arcsec, and find a total of 42,420 stars in common between APOGEE DR14 and LAMOST DR3. For this study we used the APOGEE flag called *ASPCAPFLAG*, to remove stars where any of the *TEFF*, *LOGG*, *CHI2*, *COLORTE*, *ROTATION*, *SNR* flags are set (see Holtzman et al. 2015 and García Pérez et al. 2016 for full details on the different flags used in APOGEE data). This leaves 41,547 objects in the APOGEE - LAMOST stellar catalog.

2.1. Sky coverage and magnitude range

In Figure 1 we show the Galactic coordinates of the APOGEE-LAMOST stellar catalog in a Hammer-Aitoff projection. Because of the Northern Hemisphere location of LAMOST and the SDSS-telescope APOGEE used for DR12 and DR14, most of the common stars lie in the Galactic anti-center and in the North Galactic Cap.

There are also common targets in the *Kepler* field, where the spectroscopic parameters provided by the APOGEE project are complemented with asteroseismic surface gravities, masses, radii, and mean densities determined by members of the Kepler Asteroseismology Science Consortium (KASC) (Pinsonneault et al. 2014). There are similar efforts within the LAMOST collaboration in the *Kepler* fields (Ren et al. 2016).

Figure 2 shows the H -band luminosity distribution for the APOGEE - LAMOST stellar catalog compiled in this study. Most stars in common between APOGEE and LAMOST are in the magnitude range from 9 to 12 in the H -band.

¹ <http://dr3.lamost.org/>

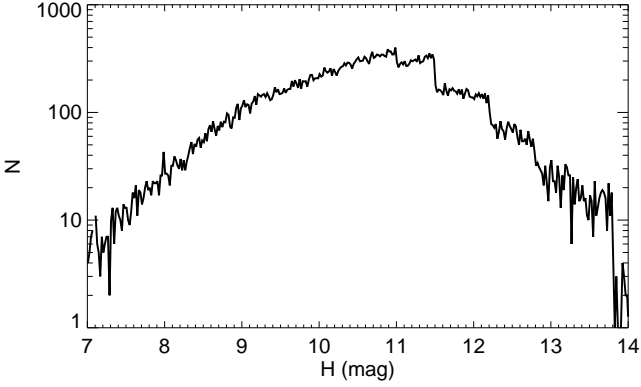


Fig. 2. Luminosity distribution function in the H -band for the APOGEE - LAMOST stellar catalog. The catalog covers a large magnitude range from 7 to almost 14 mag. Most of the stars are in the magnitude range from 9 to 12 in the H -band.

2.2. Signal-to-noise ratio (SNR)

APOGEE aims to obtain high-resolution, high SNR (> 100 per half resolution element of pixels), H -band spectra for stars in the bulge, disk, and halo of the Milky Way (Zasowski et al. 2013, Zasowski et al. 2017). Most APOGEE targets are observed in several visits. After multiple visits, a combined spectrum is produced (Nidever et al. 2015). LAMOST DR3 provides the SNR-per-pixel for the targets as calculated in five different bands, u , g , r , i and z , respectively. Using the center wavelength and bandwidth, they obtain the wavelength range for each SDSS band, and then the SNR in each band is the median value at each pixel in this band (Luo et al. 2015). The cumulative histograms of SNR in APOGEE and in LAMOST for the z -band (left panel in Fig. 3) shows that the APOGEE survey has 80% of the in common stars with SNR > 100 , and 40% with SNR > 200 . The LAMOST survey has 40% of the in common stars with SNR > 100 , and 10% with a SNR > 200 ². The right panel in Figure 3 shows the SNR from APOGEE and LAMOST spectra for the common stellar catalog as a function of the H -band magnitude from the 2MASS survey (Skrutskie et al. 2006). This figure shows a clear relation between magnitude and SNR in APOGEE. This relation is weaker in LAMOST DR3 data and the H -band, where a given stellar magnitude has a wide range in SNR.

2.3. Radial velocities

In APOGEE DR14 (Abolfathi et al. 2018) radial velocities (RVs) are determined for each individual visit to identify stars with companion-induced Doppler shifts. The individual visit spectra are resampled and combined to generate a single spectrum for each object. Final RVs are obtained by cross-correlation against a grid of synthetic spectra spanning a wide range of stellar parameters. The APOGEE instrument and the existing radial velocity software routinely deliver radial velocities per visit at a precision of $\sim 0.07 \text{ km s}^{-1}$ for SNR > 20 , while the survey provides external calibration sufficient to ensure accuracies at the level of $\sim 0.35 \text{ km s}^{-1}$. RVs in APOGEE are reported with

² APOGEE SNR is not real for SNR $> 200 - 300$ since it is obtained from the photon shot noise. At very high SNR it becomes limited by the detector flatfielding, artifacts and telluric/sky lines.

respect to the center of mass (barycenter) of the solar system (Nidever et al. 2015).

The LAMOST 1D pipeline (Luo et al. 2015) also measures the RVs by using a cross-correlation method. The pipeline recognizes the stellar spectral classes and simultaneously determines the RVs from the best fit correlation function between the observed spectra and the template. The RVs are corrected from geocentric coordinates to barycentric coordinates. Figure 4 shows the mean reported RV uncertainties with respect to the mean SNR for the common catalog between APOGEE and LAMOST. Figure 4 shows the standard deviation of the SNR and the error deviation of σ_{RV} for bins of 3,000 stars by SNR. Nearly all the stars in the APOGEE catalog in common with LAMOST have $\sigma_{RV} < 0.1 \text{ km s}^{-1}$. For stars with $\text{SNR}_{\text{APOGEE}} > 100$, APOGEE determines $\sigma_{RV} < 0.03 \text{ km s}^{-1}$. The LAMOST calculated RV uncertainties for stars in common with APOGEE range from 3.5 to 18 km s^{-1} , depending on the SNR. Stars with $\text{SNR}_{\text{LAMOST}} > 100$, show $\sigma_{RV} < 8 \text{ km s}^{-1}$ (see Fig. 4).

In Figure 5 we have the histogram of discrepancies between APOGEE and LAMOST RVs. The discrepancies show a clear offset of $4.54 \pm 0.03 \text{ km s}^{-1}$, with a dispersion of 5.8 km s^{-1} . Most of the scatter in the discrepancies is expected to come from LAMOST RVs uncertainties (Fig. 4), which suggests that the average LAMOST measurement error for the RVs is $\sim 6 \text{ km s}^{-1}$. This is consistent with the median in the reported RV LAMOST uncertainty, where the value is $\sim 6.5 \text{ km s}^{-1}$. Huang et al. (2015) compared 499 RVs from LAMOST DR1 with RVs of the same targets derived from MMT+Hectospec, and also found an offset, in their case of $3.8 \pm 0.3 \text{ km s}^{-1}$. Furthermore, a similar offset appears between an external comparison between LAMOST DR1 and SEGUE DR9 for common objects, where the result is $< \Delta \text{RV} > = 7.2 \text{ km s}^{-1}$. A similar offset is also reported in Schönrich & Aumer (2017) for the LAMOST survey.

In Figure 6 we explore the mean RVs discrepancies as a function of $< \text{SNR} >$, $< T_{\text{eff}} >$, $< [\text{Fe}/\text{H}] >$ and $< \log g >$ from APOGEE DR14. We find no clear systematic trends between the RVs discrepancies and the stellar parameters, except for a weak trend of amplitude 1 km s^{-1} as a function of $< [\text{Fe}/\text{H}] >$ (lower-left panel in Fig. 6). From the lack of trends in what we are able to compare between the datasets, the origin of the global RV offset between the surveys is unclear.

2.4. Stellar atmospheric parameters

Stellar parameters are derived from the combined APOGEE spectra with the APOGEE Stellar Parameters and Chemical Abundances Pipeline (ASPCAP) (García Pérez et al. 2016), where an interpolated grid of synthetic spectra (e.g., Zamora et al. 2015) is searched to find the best match to each observed spectrum. ASPCAP performs a multidimensional χ^2 minimization using the code FERRE³. We emphasize that for this comparison we use APOGEE *calibrated* stellar parameters. ASPCAP derive parameters for nearly all the observed stars, but these parameters suffer for systematic errors, most likely associated to shortcomings in the models. Hence, APOGEE produce *calibrated* parameters, i.e. surface gravities calibrated to seismic gravities via asteroseismology for giant stars. We refer the reader to Holtzman et al. 2015 and García Pérez et al. 2016, where ASPCAP and calibrated parameters are explained in detail.

The LAMOST Stellar Parameter Pipeline (LASP) also determines automatically the fundamental stellar parameters from

³ github.com/callendeprieto/ferre

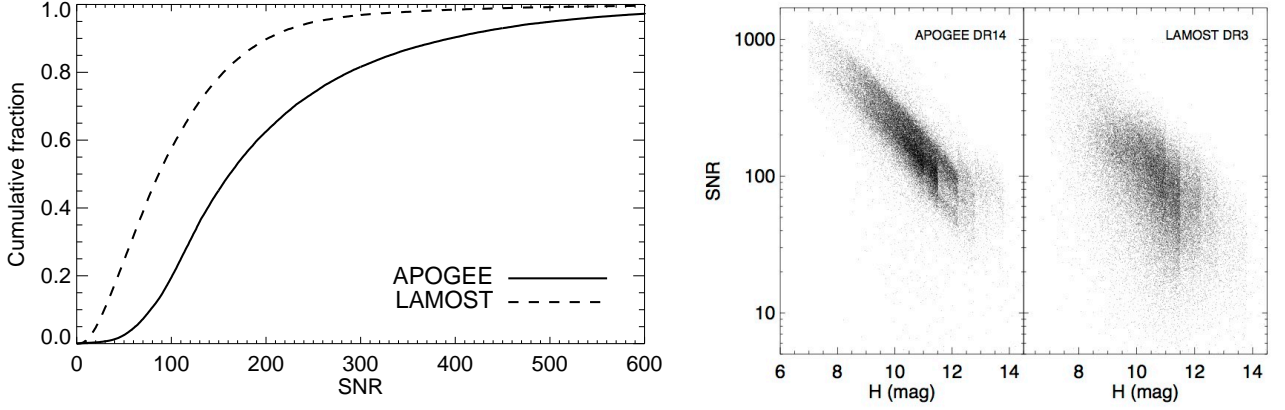


Fig. 3. Left panel: cumulative histograms of SNR-per-half resolution element (approximately a pixel) for APOGEE (solid line) and SNR-per-pixel for LAMOST (dashed line), as provided from the original catalogs. Right panels: SNR from APOGEE and LAMOST spectra for the common objects as a function of the H -band magnitude from the 2MASS survey.

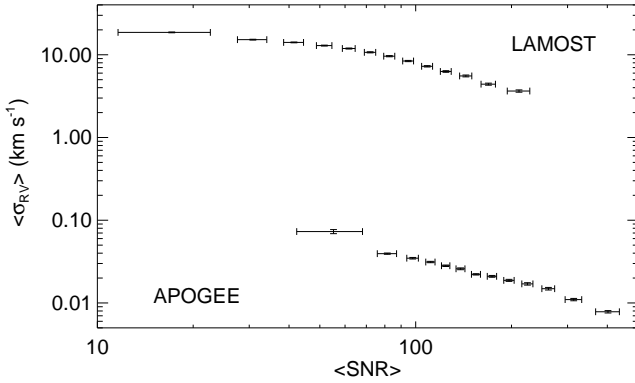


Fig. 4. Mean radial velocity uncertainties as a function of the mean SNR for the common stars in APOGEE DR14 and LAMOST DR3. Each point contains 3,000 stars. The error bars represent the standard deviation in SNR and the standard error in σ_{RV} .

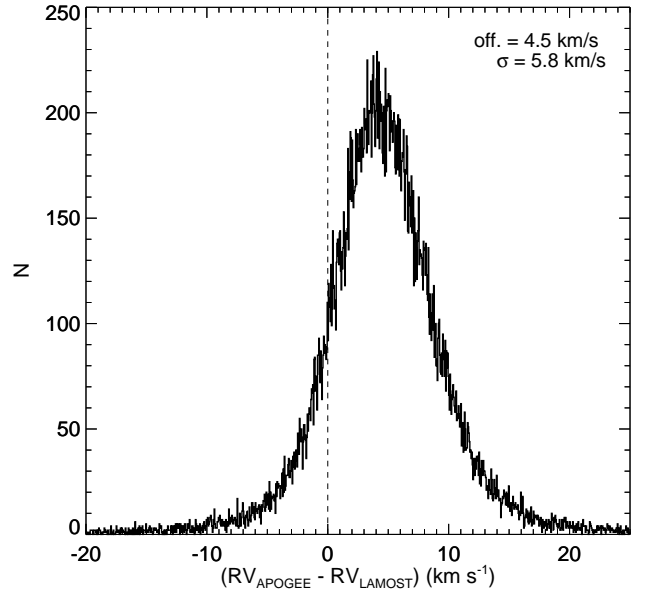


Fig. 5. Histograms of discrepancies between APOGEE and LAMOST RVs. The distribution shows a mean offset of about 5 km s^{-1} .

LAMOST spectra. LAMP adopts two methods to obtain a single set of derived stellar parameters: (i) the Correlation Function Initial (CFI) values (Du et al. 2012) followed by the ULYSS package (Wu et al. 2011) and (ii) the CFI method is used to get an initial guess for the stellar parameters, while ULYSS generates the final values from the observed spectra (Luo et al. 2015).

In Figure 7 we have the stellar atmospheric parameters for temperature, metallicity and surface gravity reported in APOGEE DR14 (black line), and in LAMOST DR3 (red line) for the APOGEE - LAMOST catalog. The histograms show the stellar parameters range we compare in this exercise. Figure 8 shows the histograms of discrepancies between derived T_{eff} , $[\text{Fe}/\text{H}]$ and $\log g$ in logarithmic scale from the APOGEE and LAMOST surveys for the objects in common. We observe a small offset in effective temperature of about 13 K, with a scatter of 155 K. We also observe a small offset in $[\text{Fe}/\text{H}]$ of about 0.06 dex together with a scatter of 0.13 dex. Using only surface gravities in calibrated red giants from APOGEE DR14, where there are 24,074 stars in common, we notice that the largest offset between both surveys occurs in the surface gravities, where a deviation of 0.14 dex is observed with a substantial scatter of 0.25 dex. Holtzman et al. (2018, in prep.) reported that at low surface gravities the APOGEE ASPCAP spectroscopy surface gravities

are systematically higher than the asteroseismic surface gravities; as a result the $\log g$ in APOGEE DR14 is calibrated using a linear surface gravity fit to the seismic $\log g$ measured for giants in the first APOKASC catalog (Pinsonneault et al. 2014). This calibration could explain the offset reported here with respect to the LAMOST surface gravities. More details about the spectroscopic and photometric NASA *Kepler* field follow-ups is given in Section 3. Figure 8 also shows that the histograms of discrepancies between the measured stellar parameters in APOGEE and LAMOST are not symmetric, which suggests that other systematic effects may be present in the data.

Figure 9 shows the $T_{\text{eff}} - \log g$ diagram from the APOGEE DR14 and LAMOST DR3 stellar parameters, color coded by $[\text{Fe}/\text{H}]$. Over-plotted are 5 Gyr isochrones (Bressan et al. 2012) at three different metallicities as indicated in the figure. There is a generally good agreement between the theoretical stellar tracks

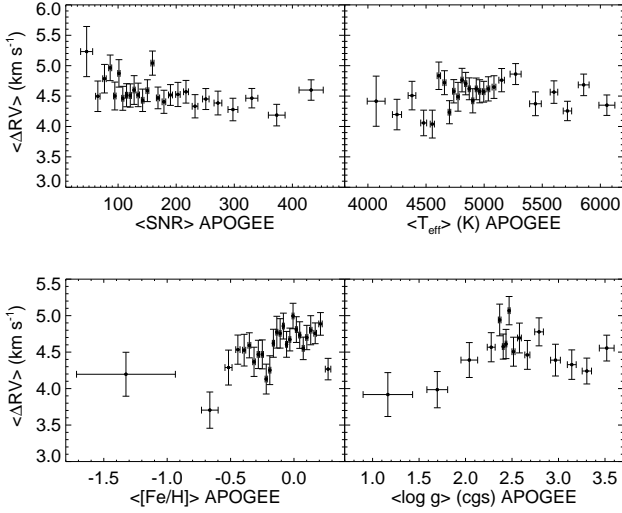


Fig. 6. Mean radial velocity discrepancies with respect to $\langle \text{SNR} \rangle$, $\langle T_{\text{eff}} \rangle$, $\langle [\text{Fe}/\text{H}] \rangle$ and $\langle \log g \rangle$ from APOGEE DR14. There is no clear systematic trends between the RVs discrepancies and the stellar parameters, where the amplitude is $\leq 1 \text{ km s}^{-1}$.

and the data-sets from both surveys. However, the Red Clump (RC) appears clearly distinct in the APOGEE $T_{\text{eff}} - \log g$ diagram around $\log g \sim 2.5$, while the clump in the LAMOST data is more diffuse, showing a spread from 2.2 to 2.7 dex in surface gravity. In the next sections we explore the reported uncertainties associated with the atmosphere stellar parameters.

2.4.1. Uncertainties

In Figure 10 we explore the quoted uncertainties in the main atmosphere stellar parameters in the APOGEE-LAMOST stellar catalog. The three panels show the reported uncertainties in T_{eff} , $[\text{Fe}/\text{H}]$ and $\log g$ as a function of the SNR for both surveys.

From the entire sample in common we calculated the mode of the reported uncertainty distribution for the three atmospheric parameters. The median APOGEE uncertainties are $\sim 90 \text{ K}$, $\sim 0.01 \text{ dex}$ and $\sim 0.06 \text{ dex}$ in T_{eff} , $[\text{Fe}/\text{H}]$ and $\log g$, respectively. For LAMOST, we find $\sim 80 \text{ K}$, $\sim 0.08 \text{ dex}$ and also $\sim 0.12 \text{ dex}$, respectively. From these later values, the reported LAMOST DR3 uncertainties seem underestimated. Interestingly, the uncertainties in the APOGEE DR14 stellar parameters are nearly independent of the SNR, asymptoting to a “floor” due to systematics. On the other hand, the uncertainties reported in the LAMOST DR3 show a clear dependence on the SNR, with no clear “floor” reached at the highest SNR. For the effective temperature, stars with $\text{SNR}_{\text{LAMOST}} > 100$ show that, on average, $\sigma_{\text{Teff}_{\text{lamost}}} < \sigma_{\text{Teff}_{\text{apogee}}}$. For iron abundances, we have that APOGEE uncertainties are, on average, lower than the iron uncertainties reported in LAMOST independent of the SNR of the spectrum, while stars with $\text{SNR}_{\text{LAMOST}} > 150$ report on average, more precise surface gravity uncertainties than those claimed for the APOGEE sample (Fig. 10). We use the histograms of discrepancies between stellar parameter to understand the true error values behind the data, where we assume that the observed scatter constrains the stellar parameter uncertainties. In Table 1 we show the mean offset determined from the histograms of discrepancies, the observed scatter and the sum of the uncertainties in both catalogs. Although, the discrepancies are not perfect Gaussians due to systematic effects in the data (see Fig. 8), we as-

sume that $\sigma \sim (\sigma_A^2 + \sigma_L^2)^{1/2}$. In Table 1 we have that for stars with $\text{SNR}_{\text{LAMOST}} > 200$, the intrinsic scatter from the discrepancies is always larger than $(\sigma_A^2 + \sigma_L^2)^{1/2}$. Moreover, we saw in Figure 10 that APOGEE stellar parameters are nearly independent of SNR. Hence we conclude that at high SNR (> 100) the uncertainties from LAMOST are underestimated.

2.4.2. Systematic effects

We use the APOGEE-LAMOST stellar catalog to explore the existence of systematic errors in the atmosphere stellar parameters derived using the respective survey stellar pipelines described above.

In Figure 11 we show the discrepancies in T_{eff} between the surveys for stars in common as a function of $\langle \text{SNR} \rangle$, $\langle T_{\text{eff}} \rangle$, $\langle [\text{Fe}/\text{H}] \rangle$ and $\langle \log g \rangle$, where every point bins 1500 stars. ΔT_{eff} has small variations with respect to the APOGEE SNR, with an amplitude smaller than 80 K. Interestingly, we observe that ΔT_{eff} changes sign for stars colder than $\sim 4500 \text{ K}$ and for stars hotter than $\sim 5200 \text{ K}$. The offset for the cold stars is around $\sim 50 \text{ K}$, however for hot stars it reaches values of 100 K (see top panels in Fig. 11). There is a clear trend between ΔT_{eff} and $\langle [\text{Fe}/\text{H}] \rangle$, where the sign of ΔT_{eff} flips at solar metallicity. There is no evident trend between $\langle \log g \rangle$ and ΔT_{eff} (see lower panels in Fig. 11).

In Figure 12 we see how the average discrepancy in $[\text{Fe}/\text{H}]$ changes with respect to the $\langle \text{SNR} \rangle$ and the main stellar parameters. There is an evident offset of $\sim 0.06 \text{ dex}$ already reported above. This offset is nearly independent of the $\langle \text{SNR} \rangle$ in the APOGEE spectra, although for stars where the $\text{SNR} < 100$ the offset goes from 0.06 to 0.1 dex (see top-left panel in Fig. 12). We also find a clear relation between $\langle T_{\text{eff}} \rangle$ and $\Delta[\text{Fe}/\text{H}]$. The metallicity offset is larger for colder stars, while for stars with $T_{\text{eff}} > 5200 \text{ K}$, $\Delta[\text{Fe}/\text{H}] \sim 0.0 \text{ dex}$ (top-right panel in Fig. 12). $\Delta[\text{Fe}/\text{H}]$ is independent of the $\langle [\text{Fe}/\text{H}] \rangle$ for the range $-0.5 < [\text{Fe}/\text{H}] < 0.5 \text{ dex}$, however there is a relation between the two quantities for stars more metal-poor than -0.5 dex . Interestingly, for stars in the surface gravity range $1.0 < \log g < 1.5$ we do not see the offset in $[\text{Fe}/\text{H}]$ (lower panels in Fig. 12).

Finally, Figure 13 shows $\Delta \log g$ as a function of the main stellar parameters from APOGEE and the average SNR. As in the previous figures each point represents 1500 stars and the errors bars are the standard error of the mean for $\log g$ and the standard deviation in the SNR. As we mentioned above there is an offset of $\sim 0.15 \text{ dex}$ in $\Delta \log g$. This offset is independent of the SNR of the observed spectra. For stars colder than 4800 K we observe a dependence between $\Delta \log g$ and T_{eff} . In the lower panels of Figure 13, $\Delta \log g$ as a function of $\langle [\text{Fe}/\text{H}] \rangle$ shows variations of about 0.1 dex. We also find a dependence between $\langle \log g \rangle$ and $\Delta \log g$ for stars with $\log g < 2.5 \text{ dex}$.

3. The NASA Kepler field

In Section 2.4 we reported a substantial offset in the surface gravity of 0.14 dex between the two surveys. We can make use of the NASA *Kepler* mission (Borucki et al. 2010) to independently check the source of the discrepancies. The *Kepler* mission has obtained high-precision photometric data over the past four years. *Kepler* data enable precise stellar astrophysics thanks to asteroseismic measures of red giants, where uncertainties in surface gravity $< 0.05 \text{ dex}$ can be derived (Mathur et al. (2017) and references therein). In the APOGEE-LAMOST stellar catalog there are 6846 stars in the *Kepler* field.

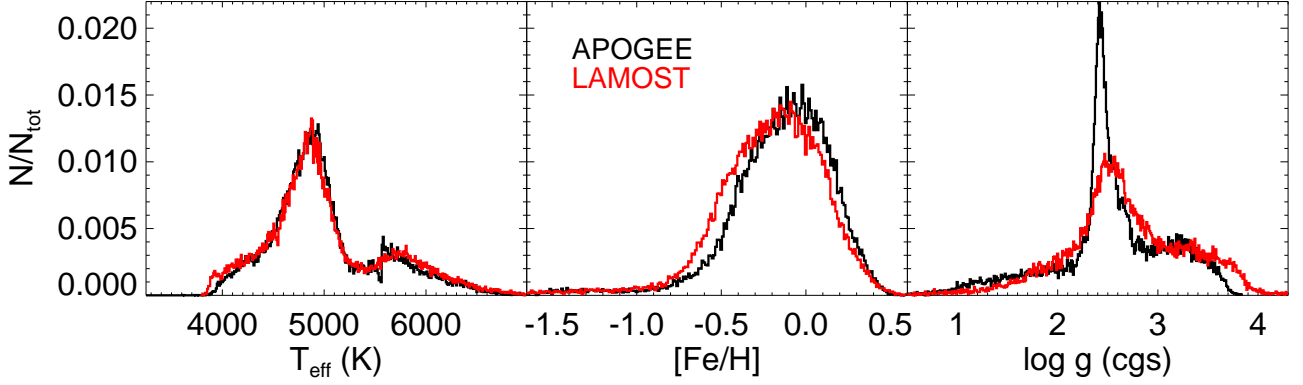


Fig. 7. Temperature, metallicity and surface gravity distribution of the APOGEE-LAMOST catalog, using the stellar parameters from APOGEE DR14 (black line), and the parameters reported in LAMOST DR3 (red line).

Table 1. Mean offset from the histogram of discrepancies, the observed scatter and the sum of uncertainties in both catalogs for different SNR range in the LAMOST survey.

| SNR _L | $\langle \Delta T_{\text{eff}} \rangle$ | $\sigma_{T_{\text{eff}}}$ | $(\sigma_{\text{A}}^2 + \sigma_{\text{L}}^2)^{1/2}$ | $\langle \Delta[\text{Fe}/\text{H}] \rangle$ | $\sigma_{[\text{Fe}/\text{H}]}$ | $(\sigma_{\text{A}}^2 + \sigma_{\text{L}}^2)^{1/2}$ | $\langle \Delta \log g \rangle$ | $\sigma_{\log g}$ | $(\sigma_{\text{A}}^2 + \sigma_{\text{L}}^2)^{1/2}$ |
|------------------|---|---------------------------|---|--|---------------------------------|---|---------------------------------|-------------------|---|
| < 100 | -2.92 | 146.82 | 191.58 | 0.07 | 0.13 | 0.15 | -0.13 | 0.25 | 0.25 |
| > 200 | -30.09 | 119.47 | 97.28 | 0.05 | 0.09 | 0.03 | -0.17 | 0.21 | 0.07 |

Table 2. Average discrepancies and standard deviations in the main stellar parameters for stars in common between APOGEE - SAGA (588 stars), and LAMOST - SAGA (312 stars) in the *Kepler* field.

| | $\langle \Delta T_{\text{eff}} \rangle$ | $\sigma_{T_{\text{eff}}}$ | $\langle \Delta[\text{Fe}/\text{H}] \rangle$ | $\sigma_{[\text{Fe}/\text{H}]}$ | $\langle \Delta \log g \rangle$ | $\sigma_{\log g}$ |
|---------------|---|---------------------------|--|---------------------------------|---------------------------------|-------------------|
| APOGEE - SAGA | -43.67 | 79.17 | 0.16 | 0.28 | -0.01 | 0.09 |
| LAMOST - SAGA | -43.41 | 82.56 | 0.10 | 0.31 | 0.14 | 0.15 |

The Strömgren Survey for Asteroseismology and Galactic Archaeology (SAGA) also mapped the *Kepler* field using the *uvby* Strömgren photometric system. Effective temperatures in the SAGA survey are derived using the Infrared Flux Method (IRFM). This technique uses multiband optical and infrared photometry to recover the bolometric and infrared flux of each star, from which its T_{eff} and angular diameter can be computed (Casagrande et al. 2014). The APOGEE survey contains 588 stars in common with SAGA, while LAMOST contains 312 objects. Figure 14 shows the histogram of discrepancies between APOGEE and SAGA for T_{eff} , $[\text{Fe}/\text{H}]$ and $\log g$ in black lines, and between LAMOST and SAGA (red lines). We find a small offset of -43 K in T_{eff} between APOGEE and SAGA and also between LAMOST and SAGA. This similarity between APOGEE and LAMOST T_{eff} is consistent with our earlier assessment finding in Figure 8.

There is also a consistent offset in $[\text{Fe}/\text{H}]$ of $+0.16$ dex between APOGEE and SAGA and LAMOST and SAGA, together with a substantial scatter of 0.3 dex. For the surface gravities we find a good agreement with a scatter of 0.09 dex between APOGEE and SAGA. The discrepancies between LAMOST and SAGA show a clear offset in gravities of 0.14 dex, where the comparison is dominated by red giants. In Section 2.4 we discussed how APOGEE surface gravities from spectroscopy are calibrated to seismic gravities, while the SAGA survey also uses global oscillation parameters to obtain $\log g$. We summarize our findings in Table 2.

Table 3. Surface gravity average discrepancies and its standard deviation with respect APOGEE - Mathur et al. (2017), and LAMOST - Mathur et al. (2017) in the NASA *Kepler* field.

| | $\langle \Delta \log g \rangle$ | $\sigma_{\log g}$ |
|-----------------------------------|---------------------------------|-------------------|
| APOGEE - Mathur17 | -0.03 | 0.13 |
| LAMOST - Mathur17 (dwarfs/giants) | 0.01/0.10 | 0.23/0.24 |

Recently, Mathur et al. (2017) revised stellar properties for a total number of 197,096 *Kepler* targets, where the priority list for input surface gravity comes from asteroseismology. We have 17,131 stars in common between APOGEE and Mathur et al. (2017). With LAMOST there are 32,547 objects in common with Mathur et al. We represent in Figure 15 the histogram of discrepancies for the surface gravity between APOGEE giants and LAMOST giants and dwarfs with respect to the gravities calibrated in the latter study. Additionally, in the LAMOST comparison we divided the sample in giants and dwarfs using a simple selection in $\log g$, where stars with $\log g < 3.5$ are considered to be giants. We find good agreement between $\log g$ in APOGEE and the surface gravities revised in Mathur et al. Interestingly, the surface gravity for dwarfs stars in LAMOST show an agreement with the gravities derived in Mathur et al. for the *Kepler* field, but for giants there is a clear offset and a large scatter of 0.24 dex. Calibrating LAMOST to

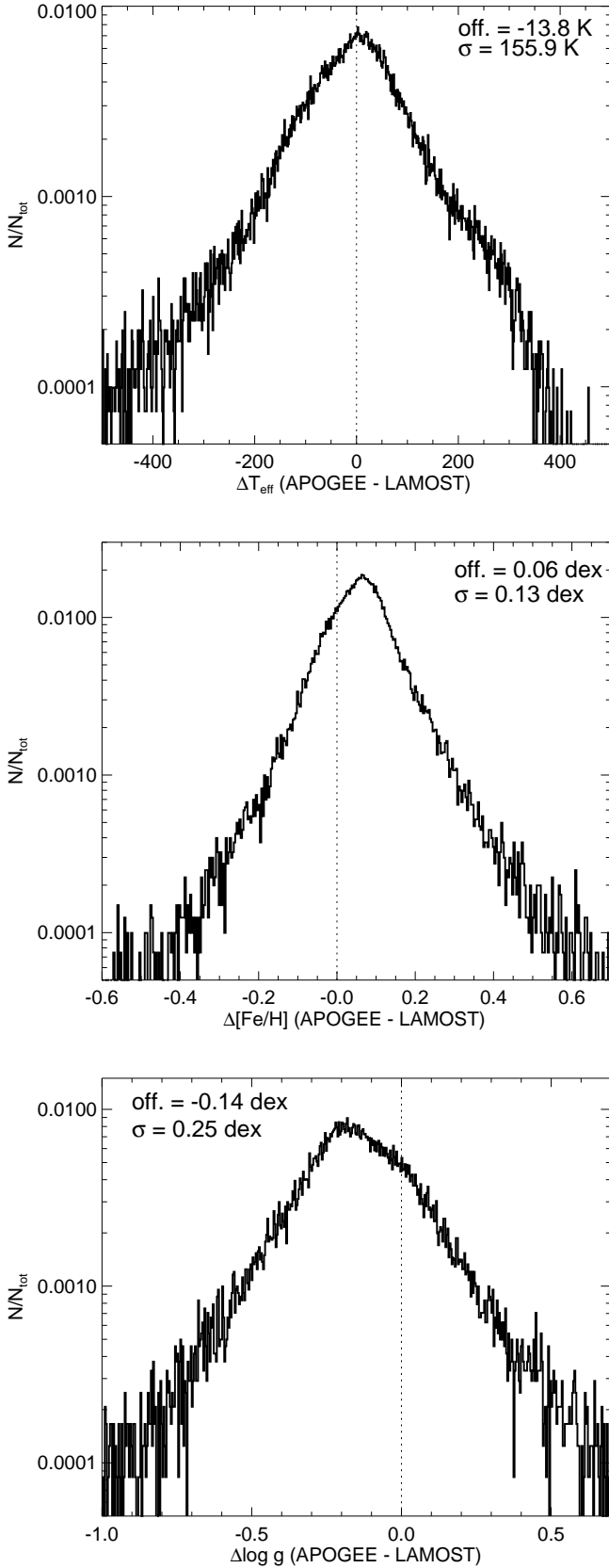


Fig. 8. Histograms of discrepancies between effective temperature (upper panel), metallicity (middle panel) and surface gravity (bottom panel) in logarithmic scale, respectively. There is a clear offset between APOGEE and LAMOST for the surface gravity, also a substantial scatter of 0.25 dex. See text for details.

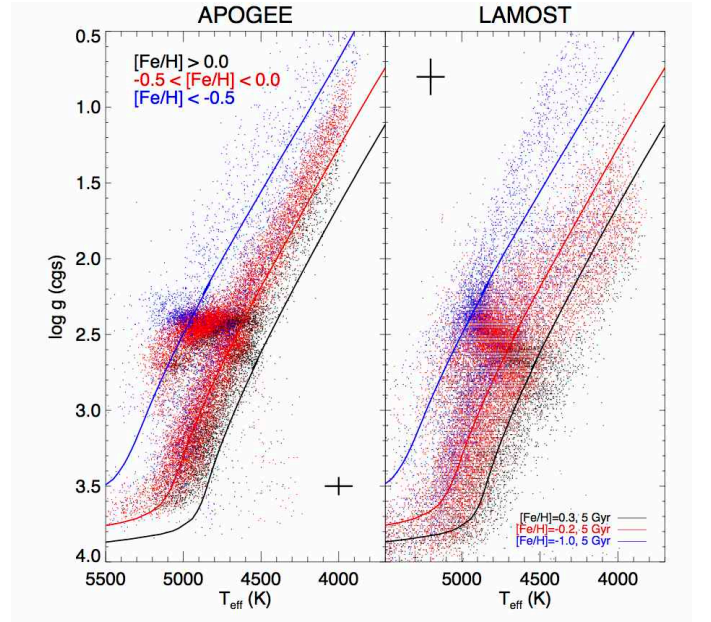


Fig. 9. $T_{\text{eff}} - \log g$ diagram from APOGEE DR14 (left) and LAMOST DR3 (right) stellar atmosphere parameters for the stars in common, color coded by three different ranges in $[\text{Fe}/\text{H}]$. Over plotted are 5 Gyr isochrones (Bressan et al. 2012) at $[\text{Fe}/\text{H}] = +0.3, -0.2$ and -1.0 dex, respectively. The errorbars represent the typical uncertainties in T_{eff} and $\log g$ in the two surveys.

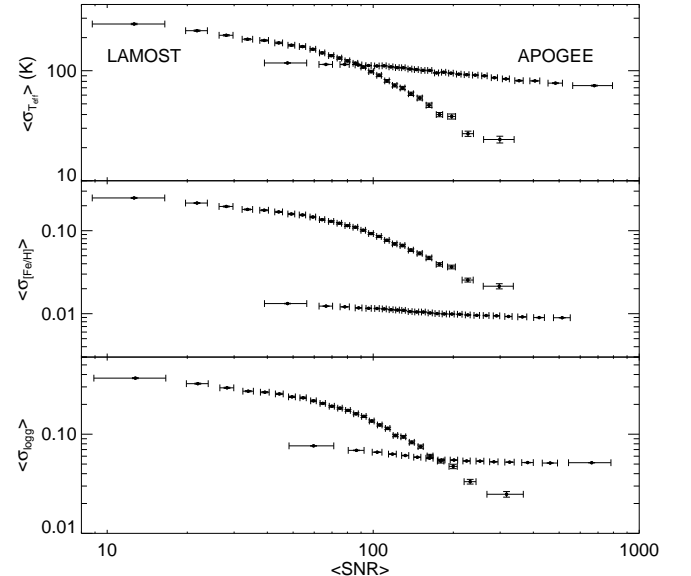


Fig. 10. Average uncertainty in T_{eff} , $[\text{Fe}/\text{H}]$ and $\log g$ as a function of the average APOGEE $\langle \text{SNR} \rangle$ for stars in common in the APOGEE and LAMOST survey. Every point has 1500 stars and the error bars represent the standard deviation in the SNR bin and the standard error of the mean for T_{eff} , $[\text{Fe}/\text{H}]$ and $\log g$, respectively.

Kepler could resolve that discrepancy. See Table 3 for simple statistics describing this comparison.

4. The Cannon on LAMOST

Ho et al. (2017) used a data-driven approach to spectral modeling, *the Cannon* (Ness et al. 2015), to transfer the calibrating

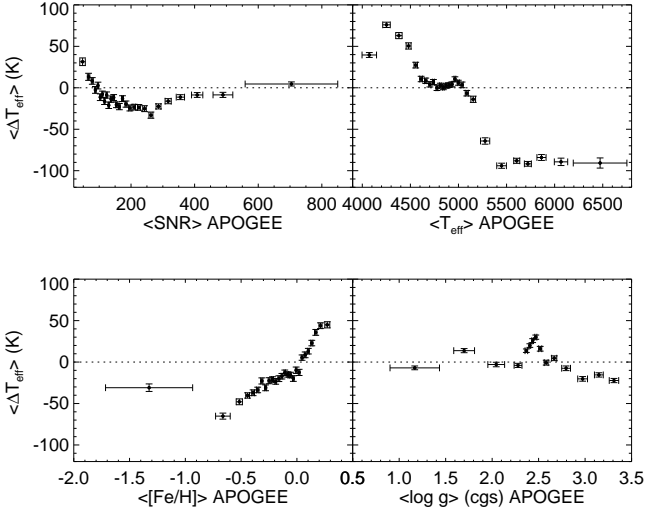


Fig. 11. Mean effective temperature discrepancies (APOGEE - LAMOST) as a function of $\langle \text{SNR} \rangle$, $\langle T_{\text{eff}} \rangle$, $\langle [\text{Fe}/\text{H}] \rangle$ and $\langle \log g \rangle$.

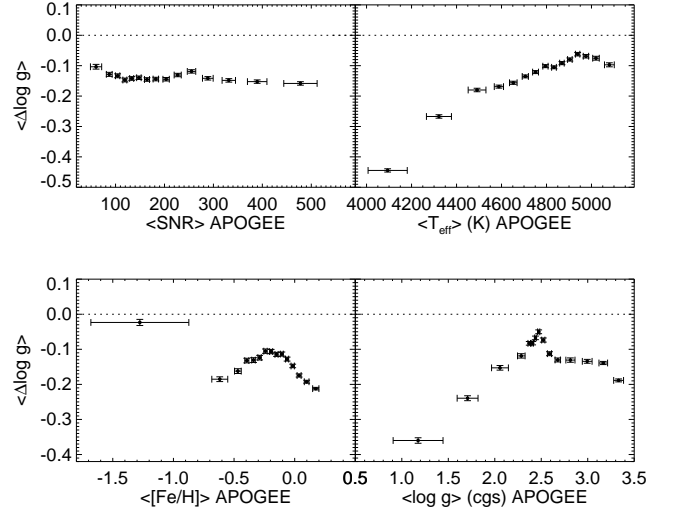


Fig. 13. Mean surface gravity discrepancies (APOGEE - LAMOST) with respect to $\langle \text{SNR} \rangle$, $\langle T_{\text{eff}} \rangle$, $\langle [\text{Fe}/\text{H}] \rangle$ and $\langle \log g \rangle$, respectively.

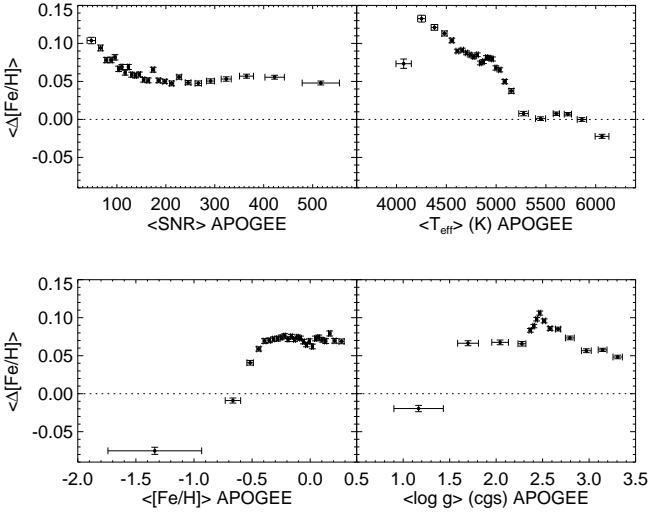


Fig. 12. Mean $[\text{Fe}/\text{H}]$ discrepancies (APOGEE - LAMOST) as a function of $\langle \text{SNR} \rangle$, $\langle T_{\text{eff}} \rangle$, $\langle [\text{Fe}/\text{H}] \rangle$ and $\langle \log g \rangle$.

information from the APOGEE survey to determine precise T_{eff} , $[\text{Fe}/\text{H}]$ and $\log g$, from the spectra of 454,180 LAMOST DR2 giants. Ho et al. (2017) select 9,952 objects common to LAMOST DR2 and APOGEE DR12 for their *training set* and these objects span a representative range of parameter space for giants (see their Fig. 4 for details), but are relatively concentrated compared to the parameter ranges explored in this paper so far. We find 17,482 stars in common between APOGEE DR14 and the catalog from Ho et al. (2017). Figure 16 shows the histogram of discrepancies between APOGEE DR14 and LAMOST/Cannon for T_{eff} , $[\text{Fe}/\text{H}]$ and $\log g$, respectively. There is a generally good agreement between the two data-sets. The offset in $[\text{Fe}/\text{H}]$ we found in Figure 8 comparing APOGEE DR14 and LAMOST DR3 is less evident in this new comparison, however the scatter remains similar. Also, the offset in $\log g$ is still present, with a scatter of ~ 0.2 dex.

We also study the behaviour of the discrepancies in the atmosphere parameters with respect to SNR, T_{eff} , $[\text{Fe}/\text{H}]$ and $\log g$. From Figure 17 we learn that the discrepancies in the stellar

parameters are nearly independent of the SNR of the APOGEE spectra. However, we find some dependence in the discrepancies of the stellar parameters with respect to T_{eff} , particularly at the coolest T_{eff} . For metal-rich stars, we also find a different trend for the $[\text{Fe}/\text{H}]$ discrepancies with respect to $[\text{Fe}/\text{H}]$ in APOGEE DR14.

A helpful exercise to understand how the different calibrations and data analysis pipelines are performing is to compare the stellar parameters from APOGEE DR12 to APOGEE DR14 versus LAMOST tied to APOGEE DR12 using *the Cannon*. Figure 18 shows the discrepancies in T_{eff} between APOGEE DR14 - APOGEE DR12 versus APOGEE DR14 - LAMOST, where the latter has been calibrated using stellar parameters from APOGEE DR12 as a reference. The figures are color-coded with respect to T_{eff} (top panels), $[\text{Fe}/\text{H}]$ (middle panels) and $\log g$ (bottom panels) from APOGEE DR14, respectively. The trends in Figure 18 show that there is a temperature and metallicity dependence in the calibration from DR12 to DR14 (Holtzman et al. in prep.). These dependences are also present in the transformation of LAMOST to APOGEE DR12 parameters space via *the Cannon*, these temperature and metallicity dependences are weaker than those observed in the transformation from DR12 to DR14. Interestingly, there is no correlation between the DR14 - DR12 discrepancies and DR14 - LAMOST tied to DR12 for T_{eff} , where a correlation would be anticipated if the parameters derived from LAMOST spectra were brought onto the APOGEE DR12 scale. More specifically, if the LAMOST parameters and abundances were perfectly tied to the APOGEE DR12 scale, we would expect to see the known differences between DR12 and DR14 imprinted on the LAMOST parameters.

In Figure 19 we have the $[\text{Fe}/\text{H}]$ discrepancies from APOGEE DR14 - DR12 and DR14 - LAMOST calibrated by DR12 via *the Cannon*. We also find no correlation between the $[\text{Fe}/\text{H}]$ discrepancies, suggesting that LAMOST/Cannon is not entirely in the APOGEE DR12 abundances space. The graphics color-coded by T_{eff} , $[\text{Fe}/\text{H}]$ and $\log g$ from DR14 also indicate that there is an $[\text{Fe}/\text{H}]$ dependence in the calibration from APOGEE DR12 to DR14.

Finally, Figure 20 shows the surface gravity discrepancies. Unlike the previous comparison, we do see a weak correlation that would suggest the mapping of LAMOST parameters

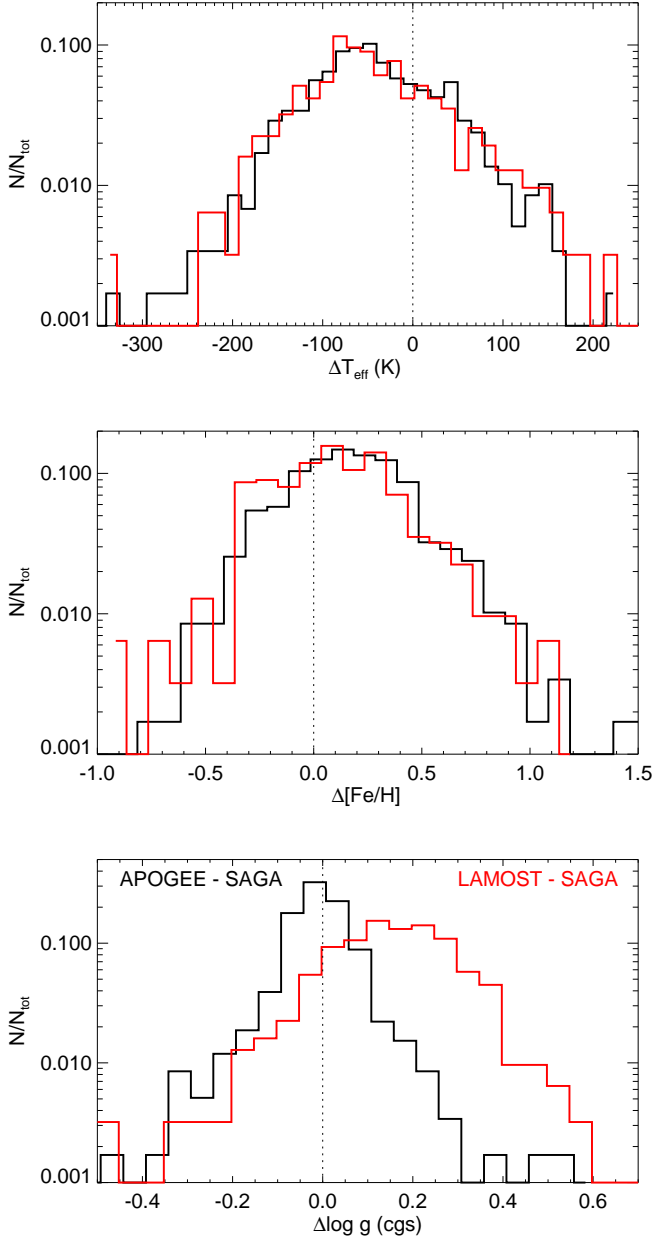


Fig. 14. Histograms of discrepancies for the main stellar atmosphere parameters between the surveys APOGEE - SAGA (black lines), and LAMOST - SAGA (red lines). See text for more details.

to APOGEE DR12. The correlation has a broad scatter and there is a stellar temperature dependency (top panel in Fig. 20). We do not observe an $[\text{Fe}/\text{H}]$ dependence in the gravity discrepancies.

5. Conclusions

In this section we summarize our findings from this exercise.

1. We created the APOGEE-LAMOST stellar catalog by combining APOGEE DR14 and LAMOST DR3, and find a total of 42,420 stars in common. Most of the common stars lie in the Galactic anti-center and in the North Galactic Cap. There are also common objects in the *Kepler* field. The luminosity distribution in the *H*-band covers a large magnitude range, from 7 to nearly 14 mag. Most of the stars

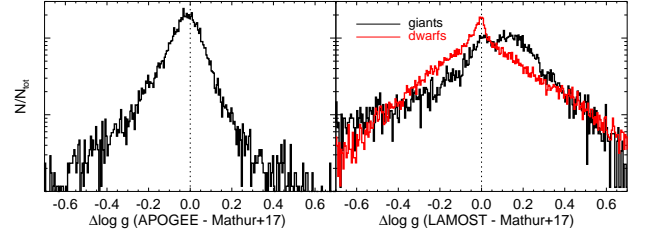


Fig. 15. Discrepancies between the surface gravity derived in APOGEE, LAMOST and Mathur et al. (2017). See text for details.

are in the magnitude range from 9 to 12 mag. We find that the APOGEE survey has 80% of these stars with $\text{SNR} > 100$, and 40% with $\text{SNR} > 200$, while the LAMOST survey has 40 per cent of stars with $\text{SNR} > 100$, and 10% with a $\text{SNR} > 200$ in the *z*-band.

2. The histogram of discrepancies between APOGEE and LAMOST RVs shows a clear offset of $4.54 \pm 0.03 \text{ km s}^{-1}$, with a scatter of 5.8 km s^{-1} . We observe that most of the scatter in the discrepancies comes from LAMOST RVs uncertainties, suggesting that the average LAMOST measurement error for the RVs is $\sim 6 \text{ km s}^{-1}$. The median reported LAMOST RV uncertainty in APOGEE-LAMOST stellar catalog is 6.5 km s^{-1} ; in good agreement with our findings in this comparison study. This seems to be a universal offset because no clear systematic trends are found between the RV discrepancies and the stellar parameters, except for a weak trend of amplitude 1 km s^{-1} as a function of $\langle [\text{Fe}/\text{H}] \rangle$.
3. We also investigate histograms of discrepancies for T_{eff} , $[\text{Fe}/\text{H}]$ and $\log g$ between the APOGEE and LAMOST surveys for the in common objects. We remind the reader that we use *calibrated* APOGEE stellar parameters, while LAMOST parameters are not calibrated. See Section 2.4 for details. We observe a small offset in the effective temperature of about 13 K, with a scatter of 155 K. A small offset in $[\text{Fe}/\text{H}]$ of about 0.06 dex together with a scatter of 0.13 dex is also found. We notice that the largest offset between both surveys occurs in the surface gravities, where a deviation of 0.14 dex is observed with a substantial scatter of 0.25 dex. The histograms of discrepancies between the measured stellar parameters in APOGEE and LAMOST are not symmetric, suggesting that other systematic effects may be present in the data. For a detailed study on the reported uncertainties we refer the reader to Section 2.4.1.
4. We use the APOGEE-LAMOST stellar catalog to explore the existence of systematic errors in the atmosphere stellar parameters. ΔT_{eff} has small variations with respect to the APOGEE SNR, where the amplitude is smaller than 80 K. We observe that ΔT_{eff} changes sign for stars colder than $\sim 4500 \text{ K}$ and for stars hotter than $\sim 5200 \text{ K}$, where the population is dominated by dwarfs. A trend between ΔT_{eff} and $\langle [\text{Fe}/\text{H}] \rangle$ is found, the sign of ΔT_{eff} flips at solar metallicity. There are no evident trends between $\langle \log g \rangle$ and ΔT_{eff} . The average discrepancy in $[\text{Fe}/\text{H}]$ varies with respect to the $\langle \text{SNR} \rangle$ and the main stellar atmosphere parameters. For example, we find a relation between $\langle [\text{Fe}/\text{H}] \rangle$ and $\Delta [\text{Fe}/\text{H}]$. Moreover, the metallicity offset is larger for colder stars, while for stars with $T_{\text{eff}} > 5200 \text{ K}$, $\Delta [\text{Fe}/\text{H}] \sim 0.0$ dex.

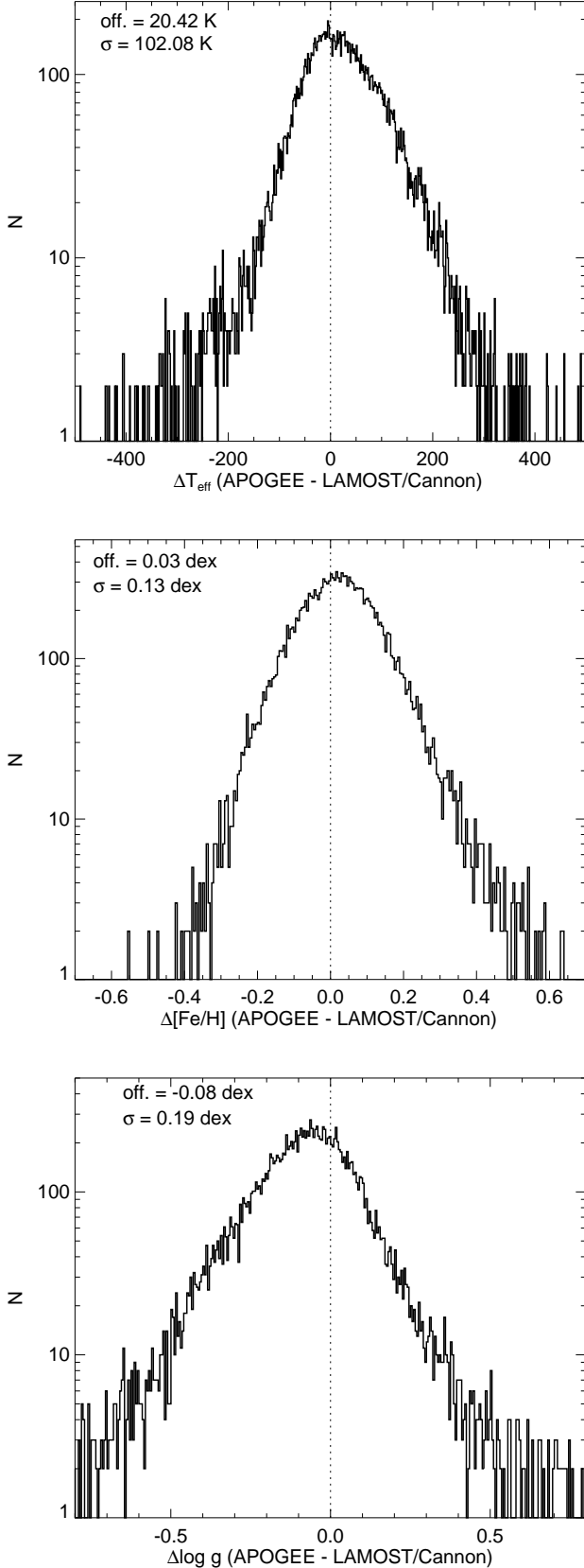


Fig. 16. Histograms of discrepancies for the main stellar atmosphere parameters between the APOGEE DR14 and LAMOST tied to APOGEE DR12 via *the Cannon*. See text for more details.

$\Delta[\text{Fe}/\text{H}]$ is independent of the $\langle[\text{Fe}/\text{H}]\rangle$ for the range $-0.5 < [\text{Fe}/\text{H}] < 0.5$ dex, however there is a relation between the two quantities for stars more metal-poor than -0.5 dex. Interestingly, for stars in the surface gravity range $1.0 < \log g < 1.5$ we do not see the offset in $[\text{Fe}/\text{H}]$. As mentioned previously, there is an offset of ~ 0.15 dex in $\Delta \log g$. This offset is independent of the SNR of the observed spectra. For stars colder than 4800 K a dependence between $\Delta \log g$ and T_{eff} is observed. The parameter $\Delta \log g$ as a function of $\langle[\text{Fe}/\text{H}]\rangle$ shows variations of about 0.1 dex. We also find a dependence between $\Delta \log g$ and $\langle \log g \rangle$ for stars with $\log g < 2.5$ dex. The reported systematic trends in T_{eff} are within the uncertainties, while the reported trends for cold, metal-poor giants are significant.

5. Mathur et al. (2017) revised stellar properties for a total of 197,096 *Kepler* targets, where the priority list for input surface gravity comes from asteroseismology. There are 17,131 stars in common between APOGEE and Mathur et al. (2017), while with LAMOST there are 32,547 objects in common. We find a good agreement between $\log g$ in APOGEE and the surface gravities revised in Mathur et al. This is expected as APOGEE surface gravities are calibrated to *Kepler* seismic $\log g$. The surface gravity for dwarfs stars in LAMOST show an agreement with the gravities derived in Mathur et al. for the *Kepler* field, while for giants there is a clear offset and a large scatter of 0.24 dex.
6. Ho et al. (2017) used *the Cannon* (Ness et al. 2015) to transfer calibrating information from the APOGEE DR12 survey to determine precise T_{eff} , $\log g$ and $[\text{Fe}/\text{H}]$ calibration for the spectra of 454,180 LAMOST giants. We find 17,482 stars in common between APOGEE DR14 and the catalog from Ho et al. (2017). There is a general good agreement between the two data-sets. The offset in $[\text{Fe}/\text{H}]$ we found comparing APOGEE DR14 and LAMOST DR3 is less evident in this new comparison, however the scatter remains similar. Also, the offset in $\log g$ is still present, with a scatter of ~ 0.2 dex, which is similar to that found between the APOGEE gravities and these found from the LAMOST/*Cannon* pipeline. We learn that the discrepancies in the stellar parameters are nearly independent of the SNR in the APOGEE spectra. However, we find dependences in the discrepancies of the stellar parameters with respect to T_{eff} . For the metal-rich stars, we also find a different trend for the $[\text{Fe}/\text{H}]$ discrepancies with respect to $[\text{Fe}/\text{H}]$ in APOGEE DR14. There is also a temperature and metallicity dependence in the calibration from DR12 to DR14. These dependences are also present in the transformation of LAMOST to APOGEE parameters space via *the Cannon*, however these temperatures and metallicity dependences are weaker than these observed in the transformation from DR12 to DR14. We report no correlation between the DR14 - DR12 discrepancies and DR14 - LAMOST tied to DR12 for T_{eff} , where a correlation should be expected if LAMOST is transferred to APOGEE DR12 correctly. We also find no correlation between the $[\text{Fe}/\text{H}]$ discrepancies, suggesting that LAMOST/*Cannon* is not entirely in the APOGEE DR12 stellar parameters space, or due to LAMOST low resolution the uncertainties in the stellar parameters are large. We also report a $[\text{Fe}/\text{H}]$ dependence in the calibration applied in the stellar parameters from APOGEE DR12 to DR14. We find a weak correlation between APOGEE DR14 - DR12 and LAMOST on DR12 surface gravity for stars hotter than 4800 K and in the $\log g$

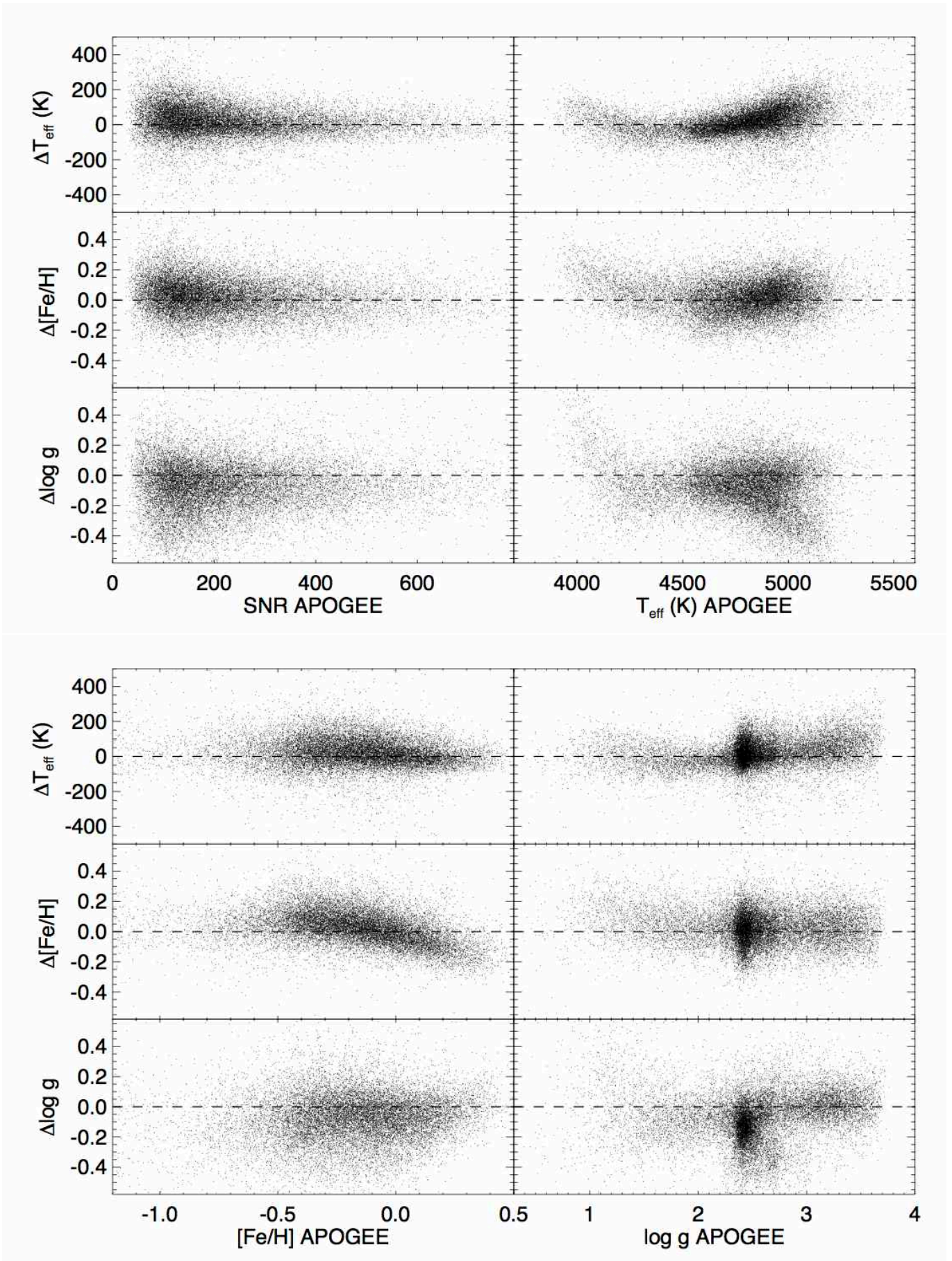


Fig. 17. Main stellar parameters discrepancies between APOGEE DR14 and LAMOST, tied to APOGEE DR12 via *the Cannon*, as a function of $\langle \text{SNR} \rangle$, $\langle T_{\text{eff}} \rangle$, $\langle [\text{Fe}/\text{H}] \rangle$ and $\langle \log g \rangle$ for stars in common.

range from 2.0 and 2.8 dex, however we do not observe an [Fe/H] dependency in the gravity discrepancies. This correlation can be explained because both catalogs use seismic gravities from *Kepler* to calibrate the surface gravity.

Zasowski, G., Johnson, J. A., Frinchaboy, P. M., et al. 2013, *AJ*, 146, 81
 Zasowski, G., Cohen, R. E., Chojnowski, S. D., et al. 2017, arXiv:1708.00155

Acknowledgements. The authors thank the anonymous referee for the useful comments and suggestions. BA and SRM acknowledge support from National Science Foundation grant AST-1616636. DAGH acknowledges support provided by the Spanish Ministry of Economy and Competitiveness (MINECO) under grant AYA-2017-88254-P. HJ acknowledges support from the Crafoord Foundation and Stiftelsen Olle Engkvist Byggmästare. Support for this work was provided by NASA through Hubble Fellowship grant 51386.01 awarded to R.L.B. by the Space Telescope Science Institute, which is operated by the Association of Universities for Research in Astronomy, Inc., for NASA, under contract NAS 5-26555. SzM has been supported by the Premium Postdoctoral Research Program of the Hungarian Academy of Sciences, and by the Hungarian NKFI Grants K-119517 of the Hungarian National Research, Development and Innovation Office. Funding for the Sloan Digital Sky Survey IV has been provided by the Alfred P. Sloan Foundation, the U.S. Department of Energy of Science, and the Participating Institutions. SDSS-IV acknowledges support and resources from the Center for High-Performance Computing at the University of Utah. The SDSS web site is www.sdss.org. SDSS-IV is managed by the Astrophysical Research Consortium for the Participating Institutions of the SDSS Collaboration including the Brazilian Participation Group, the Carnegie Institution for Science, Carnegie Mellon University, the Chilean Participation Group, the French Participation Group, Harvard- Smithsonian Center for Astrophysics, Instituto de Astrofísica de Canarias, The Johns Hopkins University, Kavli Institute for the Physics and Mathematics of the Universe (IPMU) / University of Tokyo, Lawrence Berkeley National Laboratory, Leibniz-Institut für Astrophysik Potsdam (AIP), Max-Planck-Institut für Astronomie (MPIA Heidelberg), Max-Planck-Institut für Astrophysik (MPA Garching), Max-Planck-Institut für Extraterrestrische Physik (MPE), National Astronomical Observatories of China, New Mexico State University, New York University, University of Notre Dame, Observatorio Nacional / MCTI, The Ohio State University, Pennsylvania State University, Shanghai Astronomical Observatory, United Kingdom Participation Group, Universidad Nacional Autónoma de México, University of Arizona, University of Colorado Boulder, University of Oxford, University of Portsmouth, University of Utah, University of Virginia, University of Washington, University of Wisconsin, Vanderbilt University, and Yale University.

References

- Abolfathi, B., Aguado, D. S., Aguilar, G., et al. 2018, *ApJS*, 235, 42
 Anguiano, B., Zucker, D. B., Scholz, R.-D., et al. 2015, *MNRAS*, 451, 1229
 Borucki, W. J., Koch, D., Basri, G., et al. 2010, *Science*, 327, 977
 Bressan, A., Marigo, P., Girardi, L., et al. 2012, *MNRAS*, 427, 127
 Casagrande, L., Silva Aguirre, V., Stello, D., et al. 2014, *ApJ*, 787, 110
 García Pérez, A. E., Allende Prieto, C., Holtzman, J. A., et al. 2016, *AJ*, 151, 144
 Ho, A. Y. Q., Ness, M. K., Hogg, D. W., et al. 2017, *ApJ*, 836, 5
 Holtzman, J. A., Shetrone, M., Johnson, J. A., et al. 2015, *AJ*, 150, 148
 Huang, Y., Liu, X.-W., Yuan, H.-B., et al. 2015, *MNRAS*, 449, 162
 Deng, L.-C., Newberg, H. J., Liu, C., et al. 2012, *Research in Astronomy and Astrophysics*, 12, 735
 Du, B., Luo, A., Zhang, J., Wu, Y., & Wang, F. 2012, *Proc. SPIE*, 8451, 845137
 Lee, Y. S., Beers, T. C., Sivarani, T., et al. 2008, *AJ*, 136, 2050
 Luo, A.-L., Zhao, Y.-H., Zhao, G., et al. 2015, *Research in Astronomy and Astrophysics*, 15, 1095
 Majewski, S. R., Schiavon, R. P., Frinchaboy, P. M., et al. 2017, *AJ*, 154, 94
 Mathur, S., Huber, D., Batalha, N. M., et al. 2017, *ApJS*, 229, 30
 Ness, M., Hogg, D. W., Rix, H.-W., Ho, A. Y. Q., & Zasowski, G. 2015, *ApJ*, 808, 16
 Nidever, D. L., Holtzman, J. A., Allende Prieto, C., et al. 2015, *AJ*, 150, 173
 Pinsonneault, M. H., Elsworth, Y., Epstein, C., et al. 2014, *ApJS*, 215, 19
 Ren, A., Fu, J., De Cat, P., et al. 2016, *ApJS*, 225, 28
 Schönrich, R., & Aumer, M. 2017, *MNRAS*, 472, 3979
 Skrutskie, M. F., Cutri, R. M., Stiening, R., et al. 2006, *AJ*, 131, 1163
 Smolinski, J. P., Lee, Y. S., Beers, T. C., et al. 2011, *AJ*, 141, 89
 Wilson, J. C., Hearty, F., Skrutskie, M. F., et al. 2010, *Proc. SPIE*, 7735, 77351C
 Wu, Y., Luo, A.-L., Li, H.-N., et al. 2011, *Research in Astronomy and Astrophysics*, 11, 924
 Zamora, O., García-Hernández, D. A., Allende Prieto, C., et al. 2015, *AJ*, 149, 181
 Zhao, G., Zhao, Y.-H., Chu, Y.-Q., Jing, Y.-P., & Deng, L.-C. 2012, *Research in Astronomy and Astrophysics*, 12, 723

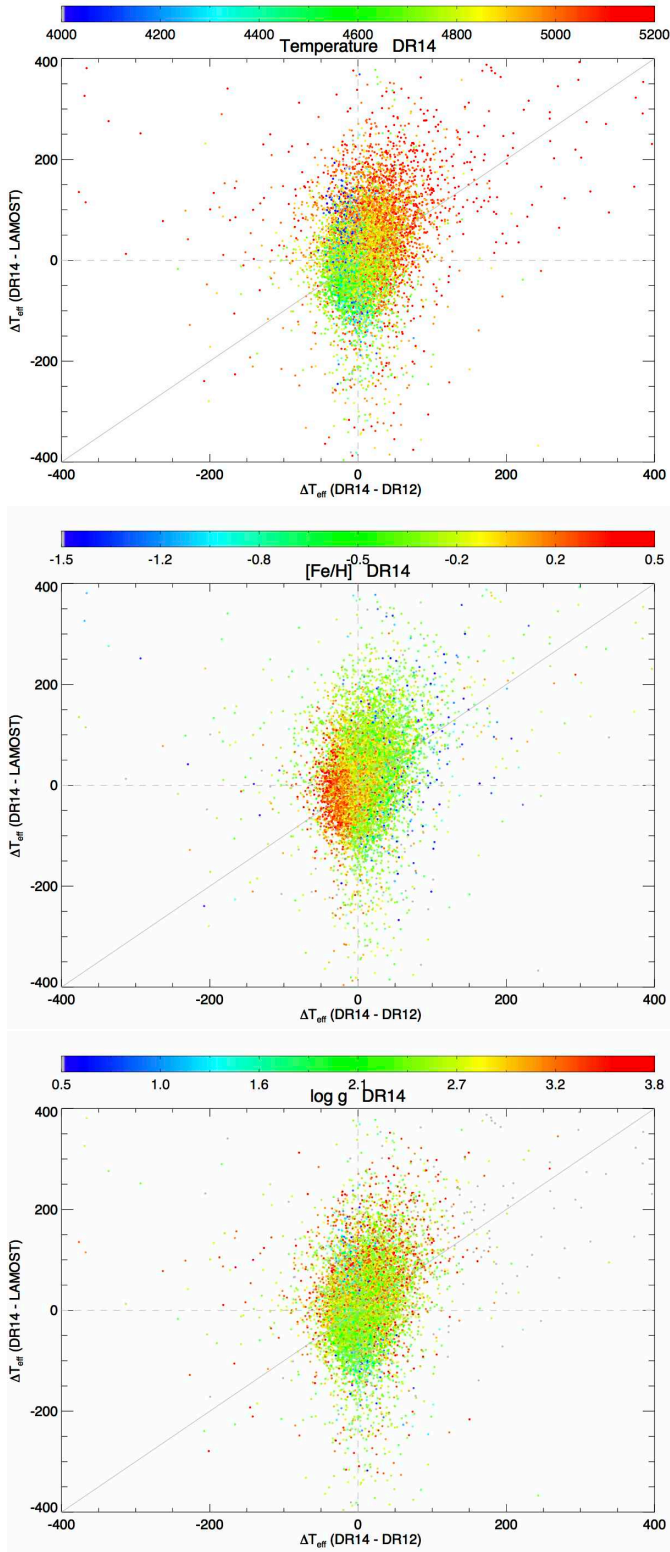


Fig. 18. T_{eff} discrepancies between APOGEE DR14 and DR12 with respect to APOGEE DR14 and LAMOST on the APOGEE DR12 stellar parameters space. The three graphics are color-coded by T_{eff} , $[\text{Fe}/\text{H}]$ and $\log g$ from APOGEE DR14.

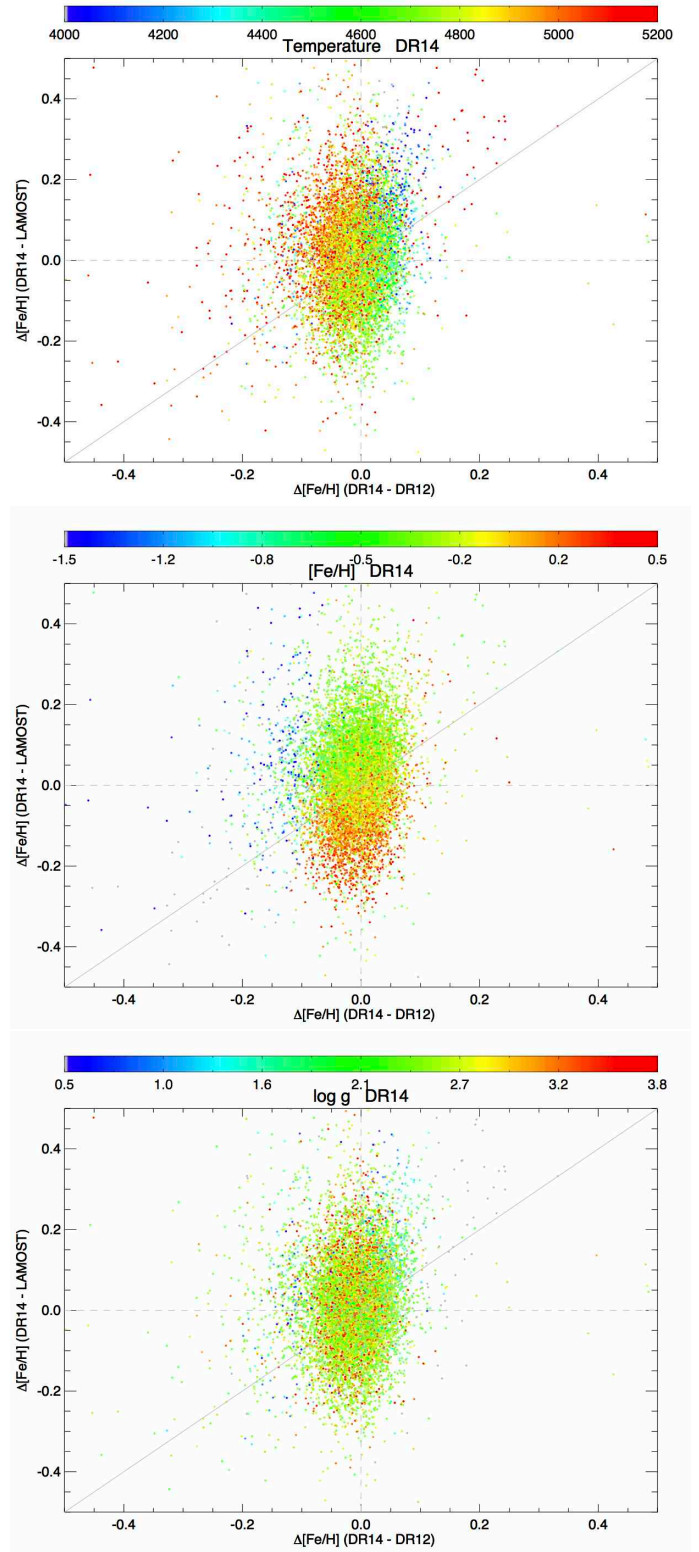


Fig. 19. $[\text{Fe}/\text{H}]$ discrepancies between APOGEE DR14 and DR12 with respect to APOGEE DR14 and LAMOST on the APOGEE DR12 stellar parameters space. The three graphics are color-coded by T_{eff} , $[\text{Fe}/\text{H}]$ and $\log g$ from APOGEE DR14.

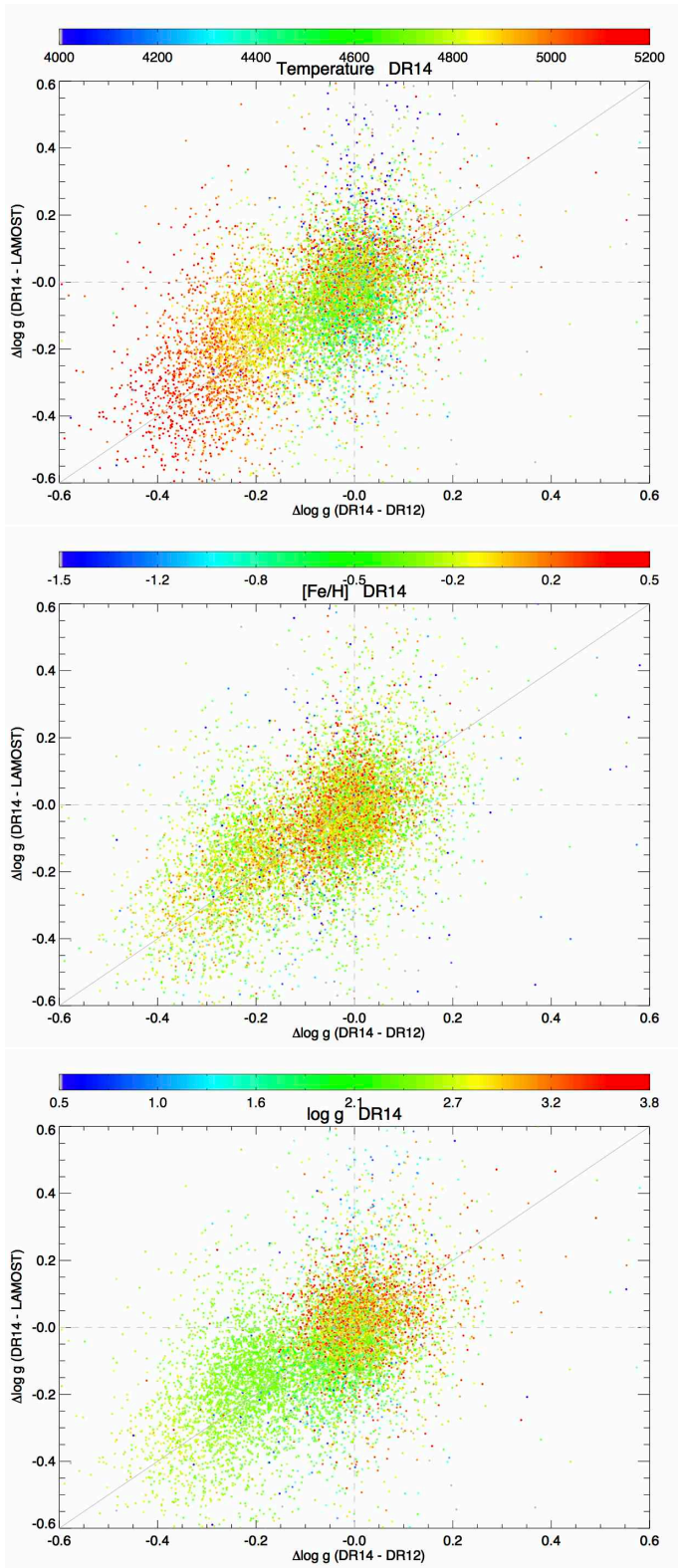


Fig. 20. Surface gravity discrepancies between APOGEE DR14 and DR12 with respect to APOGEE DR14 and LAMOST on the APOGEE DR12 stellar parameters space. The three graphics are color-coded by T_{eff} , $[\text{Fe}/\text{H}]$ and $\log g$ from APOGEE DR14.